International Journal of Heat and Mass Transfer 130 (2019) 9–24

Contents lists available at ScienceDirect

International Journal of Heat and Mass Transfer

journal homepage: www.elsevier.com/locate/ijhmt

Experimental study on fluid flow and heat transfer characteristics of falling film over tube bundle

Wei-Mon Yan [a,b,*], Chun-Wei Pan [a,b], Tien-Fu Yang [a,b], Mohammad Ghalambaz [c]

[a] Department of Energy and Refrigerating Air-Conditioning Engineering, National Taipei University of Technology, Taipei 10608, Taiwan
[b] Research Center of Energy Conservation for New Generation of Residential, Commercial, and Industrial Sectors, National Taipei University of Technology, Taipei 10608, Taiwan
[c] Department of Mechanical Engineering, Dezful Branch, Islamic Azad University, Dezful, Iran

ARTICLE INFO

Article history:
Received 1 August 2018
Received in revised form 12 October 2018
Accepted 15 October 2018
Available online 22 October 2018

Keywords:
Falling film phenomenon
Heat transfer performance
Flow behavior
Nozzles pitch

ABSTRACT

The fluid flow characteristics, film thickness and heat transfer of falling liquid films over an array of horizontal tubes are experimentally studied. The effects of the flow rate, the heat flux and nozzles-holes arrangements on the averaged convective heat transfer coefficient are addressed. An experimental setup was constructed including a water circulation system, isothermal water bath, a feeder nozzle, three horizontal test tubes, aligned vertically, the setup structure frame and measuring system. The tubes wall temperatures were measured using K-type thermocouples embedded in the test tube walls. The fluid flow and the film thickness were captured using a high-speed camera. The measurements were performed at 20 °C for two kinds of nozzles-holes configurations of single space (nozzles pitch of 12 mm) and double space (nozzles pitch of 24 mm), three flow rates of 50, 100 and 150 mLPM and four heat fluxes of 5, 10, 15 and 20 kW/m^2 °C. The measured results are reported in the form of flow-behavior photos in various time consequences, and the steady state film thickness in photos with marked measures. The tubes wall temperatures and heat flux are reported in tables and graphs. The measured results demonstrate that the arrangement of nozzles induces significant impact on the fluid flow and heat transfer characteristics of the test tubes. However, in the case of low flow rate (50 mLPM), the differences on the thermal performance are not notable. The results also show that the type and shape of film formation over the test tubes are very important on the heat transfer performance. When the liquid film extends over the test tube or covers it, the heat transfer rate increases. The heat transfer coefficient (h) for the test tube 1, just below the nozzles, is the highest; then test tube 2 in the middle receives better heat transfer rate, and test tube 3 at bottom is the last with lowest heat transfer rate. The nozzles pitch is a key parameter, which allows film bonding and can be considered as a controlling parameter for heat transfer enhancement and the flow structure.

1. Introduction

Typical falling film heat exchangers, including horizontal arrays, are commonly used in some industrial processes such as desalination, chemical processing, refrigeration, and the food industry. Mainly because of its high heat transfer coefficient and low refrigerant charge, this type of heat exchanger has showed important advantages in dealing with dirt, non-condensing effects and other problems. Hassan et al. [1] reported that the falling film evaporator is mainly has been used for seawater desalination and refrigeration, in which the fluid evaporates outside the horizontal tube bundle. Recently, horizontal falling film heat exchangers have been used in many industrial applications. For instance, the conventional heat exchangers such as coil evaporators and flooded evaporators have a lot of problems with the mineral residuals, but the falling film heat exchangers are capable of removing unwanted minerals from brine.

Ribatski and Jacobi [2] stated that falling film heat exchangers have the following advantages in air conditioning and refrigeration applications. (1) The evaporation temperature is allowed to rise, and thereby, increasing the cycle efficiency, and thus the heat transfer coefficient is higher. (2) The size of the evaporator can be reduced, and thereby, reducing the material cost of the initial manufacturing and reducing the space requirements. (3) Low refrigerant charge, and thus, reducing the cost of working fluids, including the inventory of refrigerant. Despite these advantages, falling film evaporators are not widely used in refrigeration and

* Corresponding author at: Department of Energy and Refrigerating Air-Conditioning Engineering, National Taipei University of Technology, Taipei 10608, Taiwan.
E-mail address: wmyan1234@gmail.com (W.-M. Yan).

https://doi.org/10.1016/j.ijheatmasstransfer.2018.10.070
0017-9310/

Nomenclature

A	test tube heating surface area (m^2)
D	outer diameter of the test tube (mm)
F_h	drip height (mm)
h	convective heat flux coefficient ($W/m^2 \cdot K$)
I	current (Amp.)
L_H	effective heating length of the test tube (mm)
L_t	test tube length (mm)
q	test tube surface heat flux (kW/m^2)
Q	generated heat(W)
$\overline{T_w}$	average wall temperature (°C)
T_o	drip temperature (°C)
T_w	wall temperature (°C)
V	voltage (V)
$\forall$	flow rate (mLPM)
W	nozzles pitch (mm)
ΔT	temperature difference (°C)

Greek

β	circumferential angle (°)
δ	film thickness (mm)
π	mathematical constant pi

Subscript

H	heater
h	height
o	drip outlet
t	test tube
w	wall

air conditioning systems. Part of the reason is that it is difficult to align the array and drip devices in the system. The tube configuration would severely affect the liquid distribution, especially in deep pipeline arrays. This problem results in reduced flow uniformity and forming of dry zones. In addition, the heat transfer surface, tube array geometry and operating strategies of the falling film heat exchangers have not been fully developed in the industry.

The flow pattern of the falling liquid on the horizontal pipes plays a very important role on the heat and mass transfer process; hence, the flow behavior is typically adjusted by controlling the flow rate and other physical parameters including the surface shape of the test tube and the type of the utilized fluid. These complexities have received widespread attention from many researchers and there are many studies providing valuable contributions. Among these studies, Subramaniam and Garimella [3] showed that the fluid flow over the tube bundle is actually caused by droplets between the corrugated membranes on the surface of the tube. The formation and separation of these droplets has a considerable effect on the heat transfer of the tubes. Fujita and Tsutsui [4] drenched the refrigerant on two smooth horizontal tubes arranged on the top and bottom, and then continuously increased the flow rate of the film after the flow was observed. The flow rate was divided into A-E categories in which A is a discontinuous droplet flow, B is a droplet flow, C is a columnar flow, D is a disordered columnar flow, and E is a sheet flow. After that, Armbruster and Mitrovic [5] proposed three drip modes of A-C in which A is the droplet flow, B is the column flow, and C is the flake flow. Later, Jafar et al. [6] studied the falling film transition and heat transfer on horizontal circular cylinders. The results showed that reducing the cylinder diameter leads to an increase in the heat transfer coefficient. Besides, for a completely wet surface, the heat flux has no significant effect on the heat transfer coefficient.

Sun et al. [7] indicated when the water falls on the horizontal pipes, the velocity distributions of the upper and lower parts of the pipe are asymmetric, and the flow characteristics of the top pipes are different from those of the bottom pipes. The film thickness depends on the flow rate and the angle. Hou et al. [8] utilized a displacement micrometer to experimentally determine the distribution characteristics of the film thickness around the horizontal tube. They found that the film thickness showed an asymmetric distribution around the periphery of the horizontal tube. The circumferential angle, the tube spacing, and the Reynolds number mainly affect the distribution characteristics. However, the outer diameter has almost no effect on the film thickness distribution. The minimum thickness of the film at different circumferential angles is in the range of 90–115°.

In 2014, Qiu et al. [9] simulated the characteristics of the water film outside a tube of a horizontal tube drip evaporator. They studied several factors affecting the thickness of the liquid film. The results disclosed that the film thickness first decreases from the top of the tube in the circumference direction and then increases after reaching a minimum value near the angle of 120°. Finally, due to the combined effects of gravity and surface tension, the liquid collapses at the bottom of the tube. Moreover, in a certain circumferential direction, the film thickness decreases as the flow rate decreases. When the flow rate is less than a certain value, the liquid film cannot be formed successfully, and a local drying zone may be generated on the surface of the round pipe, which should be avoided in practical designs. The film thickness decreases with increasing diameter in a certain circumferential direction. When the diameter is small, it fluctuates sharply along the tube. As the diameter increases, the liquid film distribution is uniform. With the increase of Reynolds number, the fluctuation of the falling film and the film thickness of a certain circumferential angle increase, and the growth rate is approximately linear. Chen et al. [10] measured the film thickness of a drip columnar flow by laser plus fluorescence technique. The measured results show that the film thickness increases with the increase of Reynolds number. In addition, in the axial direction, the film thickness increases with distance from the central portion of the liquid column and is maximum in the middle of two adjacent liquid columns. The maximum liquid film thickness is more than twice of its minimum value. Li et al. [11] indicated that the maximum film thickness in the droplet flow mode is equal to twice of the minimum film thickness in the axial direction. A regular peak distribution can be observed in the column flow and the sheet flow modes. Moreover, the film distribution hardly changes with time. Simulation results of Chen et al. [12] indicated that the observed flow patterns are droplets, droplet flow-column flow, columnar flow, columnar-sheet flow and sheet flow. Different flow patterns are affected by many factors, such as nozzle type, pipe diameter, tube spacing, and solution properties.

Qiu et al. [13] simulated the columnar flow and found that in the case of a single liquid column, a saddle-shaped diffusion liquid film was formed along the axial direction, and the maximum extension distance of the liquid film was obtained in axial direction. In contrast, there are lot of flow fluctuations due to the interaction between the columns when there are two adjacent liquid columns. A high peak is formed between the two columns, and the maximum film thickness is three fold larger than its minimum thickness. Besides, the film thickness of the circumferential angle is between 20 and 60, which rapidly decreases. Then it does not

change much in the range of 60–120°, and finally rises sharply in the range of 120–150°.

Hou et al. [14] theoretically studied the flow and heat transfer characteristics of a falling film over a horizontal tube bundle in details using the computation fluid dynamic for seawater desalination applications. They concluded that their model is capable of predicting the distributions of thermal parameters in the tube-side and shell-side. Zhao et al. [15] theoretically investigated the laminar liquid film falling on a horizontal smooth tube. They found that the surface tension is the key parameter for the calculations of falling film flow behavior. They also reported correlations for estimation of the local falling film thickness on a horizontal tube. Zhao et al. [16] numerically investigated the subcooled falling film heat transfer over a horizontal smooth tube. They investigated the effects various parameters such as heat flux, film flow rate, inlet liquid temperature, liquid-distributor height and tube diameter on subcooled falling film heat transfer over the tube. They also reported a heat transfer correlation for heat transfer over the tube.

Jeong and Garimella [17] and Harikrishnan et al. [18] investigated the heat and mass transfer characteristics of falling film in a horizontal tube. Qiu et al. [19] studied the falling film distribution on the surface of a 25.4 mm horizontal-tube with the falling distance of 22 mm. Ding et al. [20] have simulated the flow behavior of falling film on horizontal tubular evaporators and absorbers. They reported that the falling film flow pattern is sensitive to the initial wetting condition. Qi et al. [21] experimentally studied the effect of plate surface temperature on the wetted area and system performance for falling liquid film. Later, Qi et al. [22] numerically and experimentally investigated the heat transfer of seawater desalination with liquid film outside an elliptical tube. They simulated the distribution of liquid film outside the elliptical and circular tubes. They found good agreement between the theoretical and experimental results for the liquid film thickness. Wang et al. [23] stated that during the horizontal-tube drip-evaporation process, the heat transfer coefficient increases with the increase of drip density and temperature difference, and the thinnest part of the liquid film on the tube occurs at 90°. Zhou et al. [24] reported that the circumferential film thickness is constantly changing. The minimum film thickness is approximately in the range of 100–140°. A dry spot is formed at the bottom of the horizontal tube. Zhang et al. [25] investigated the heat transfer of LiBr/H_2O as a refrigerant pair in a falling film absorption process. They have utilized various kind of nanoparticles made of copper, alumina and carbon nanotubes as additives. They found that the presence of nanoparticles enhances the absorption process, and the copper nanoparticles provide the best absorption enhancement. Zheng et al. [26] have studied the falling film heat transfer of water over a tube-bundle at low spray density. They treated the tube surface to be super-hydrophilic. The results show that the surface treatment can affect the flow behavior of falling film over the tubes, and the fluid behavior is under significant influence of the temperature of tubes. Huang et al. [27] have introduced converging–diverging tubes as a new shape for the tubes in falling-film heat transfer applications. They reported that converging–diverging tubes shows advantages for falling film evaporation and sensible heating when the fluid Reynolds number is large. They also noticed that the rib height of the tube is an important parameter affecting the thermal performance of the tubes.

Analysis of the available literature indicates that the important factor affecting the performance of the falling-film heat exchangers is the liquid film on the tube as it forms in different states on the horizontal tube. The flow characteristics and state of the film will determine the heat transfer performance of the tube array. The flow rate also affects the state of the liquid film and its thickness, and thereby, the liquid film would affect the heat transfer performance of tubes. The literature review shows that the effect of the distance of nozzles (nozzles arrangements) on the flow behavior and heat transfer performance of the drip heat exchangers has been not addressed yet. The present study aims to address the flow behavior, liquid thickness and heat transfer performance of single drip nozzle-hole spacing and double drip nozzles-holes spacing under different flow rates and heat fluxes.

2. Experimental setup

In the present section, an experimental setup for study of fluid flow and heat transfer of falling films over tube bundle will be introduced in details. The schematic view of the experimental setup is depicted in Fig. 1. The setup is consist of an isothermal water bath with a circulating pump, a feeder with several nozzles-holes, hot test tubes, measurement devices and a structure frame. The isothermal bath and the pump provide the flow of cold water in a series of pipes connected to drilled nozzles-holes over a stainless steel feeder. The cold water exits the feeder through four nozzles-holes. Adjustable valves are also embedded after the tank for controlling the flow of nozzles to meet the experiment parameters. Bellow the feeder, three similar test tubes are arranged vertically and mounted over a flat stainless steel plate. A very powerful support, made of stainless steel of thickness 10 mm, were utilized to perfectly fix the feeder and test tubes in their places. The discharged water leaves the feeder through the nozzles-holes and reaches the test tubes where it forms a liquid falling film over the tube, and thereby, the heat transfer occurs. The water absorbs the heat from the hot tubes and then falls into an accumulation bath under the test tubs and returns to the isothermal tank bath to complete the cycle. Next to the top test tube, a high-speed camera is placed to capture the film formation on the tube. A high-speed camera is utilized to photograph the flow phenomenon on the side of the tubes array. The manual measurement function provided by IC Measure is used to measure the film thickness using the photographs. The main part of the experimental setup, the feeder and the test tubes, are described in more details in the following Sections 2.1 and 2.2, respectively.

2.1. The dripper feeder

A rectangular stainless steel block of height 18 mm, widths 20 mm and length 100 mm is selected as the dripper feeder. Seven nozzles-holes with the equal distance of 12 mm were drilled on the feeder as seen in Fig. 2(a). The nozzles-holes are numbered from one to seven where one is next to the frame of the setup. The nozzles-holes are drilled in conical shape in order to smoothly direct the water flow into their tips. As seen in Fig. 2(b), at the entrance of each nozzle a fitting is mounted to allow each nozzle connect to the cold water pipe. The schematic of the drilled holes is also depicted in Fig. 2(c). The entrance diameter of each nozzle is 10 mm and the tip of each nozzle is 1 mm while the entrance to tip distance of the nozzle is equal to the height of the dipper feeder, i.e. 18 mm. The entrance pipes are considered order of ten times larger than the nozzle tips to ensure a uniform flow for each nozzle. The experiments were conducted for two cases of nozzle pitches with W = 12 mm space (Case I) and W = 24 mm space (Case II). For Case I, the nozzles-holes of 2–5 and for Case II the nozzle-holes of 1, 3, 5 and 7 are connected to the cold water pipe.

2.2. The test section

The test tubes of this experiment are made of red copper, and their design are shown in Fig. 3. The side and section of the tubes are shown in Fig. 3(b) and (c). Each test tube is made of length L_t = 100 mm and an outer diameter D = 19 mm. The center is

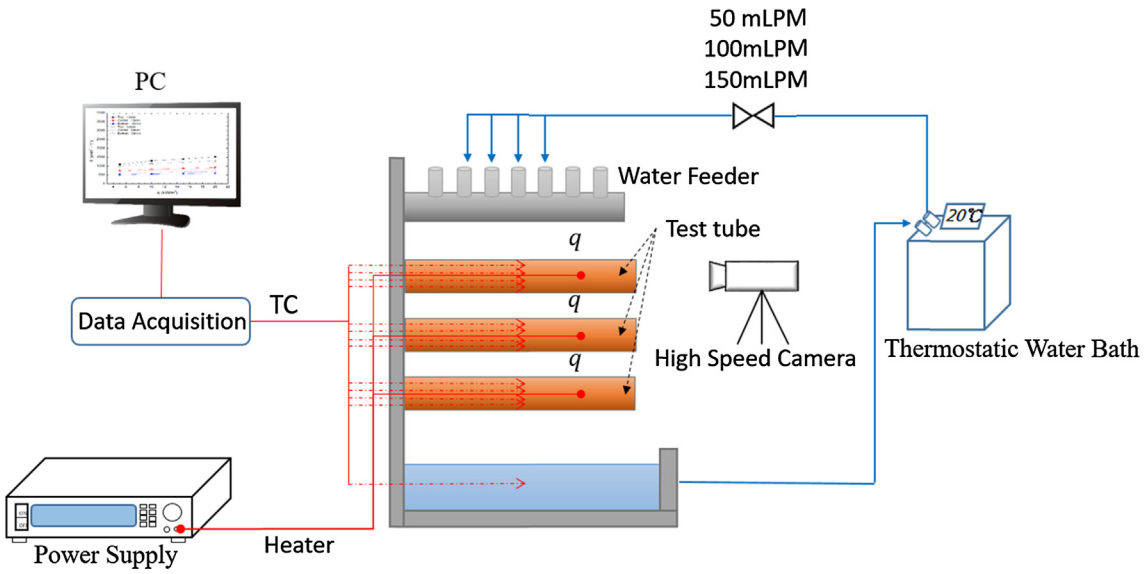

Fig. 1. Schematic view of the experimental setup.

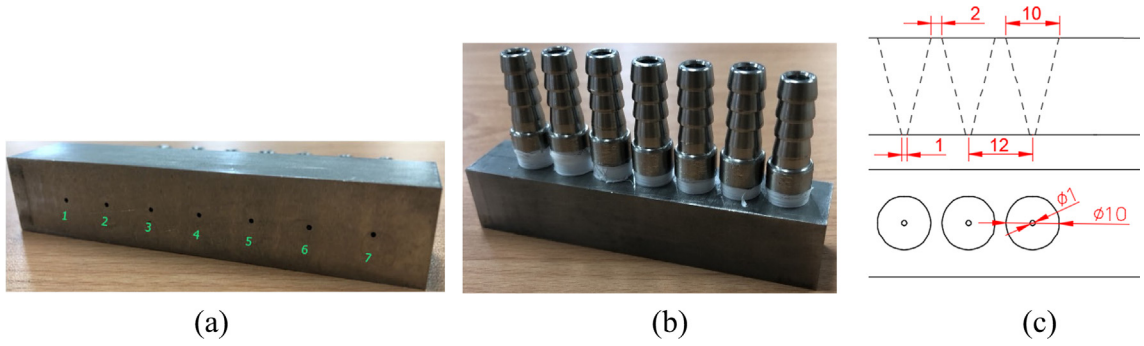

Fig. 2. The feeder and the details of the drilled holes. (a) The nozzles tips, (b) the mounting fittings, (c) the details of the drilled nozzles-holes (units in mm).

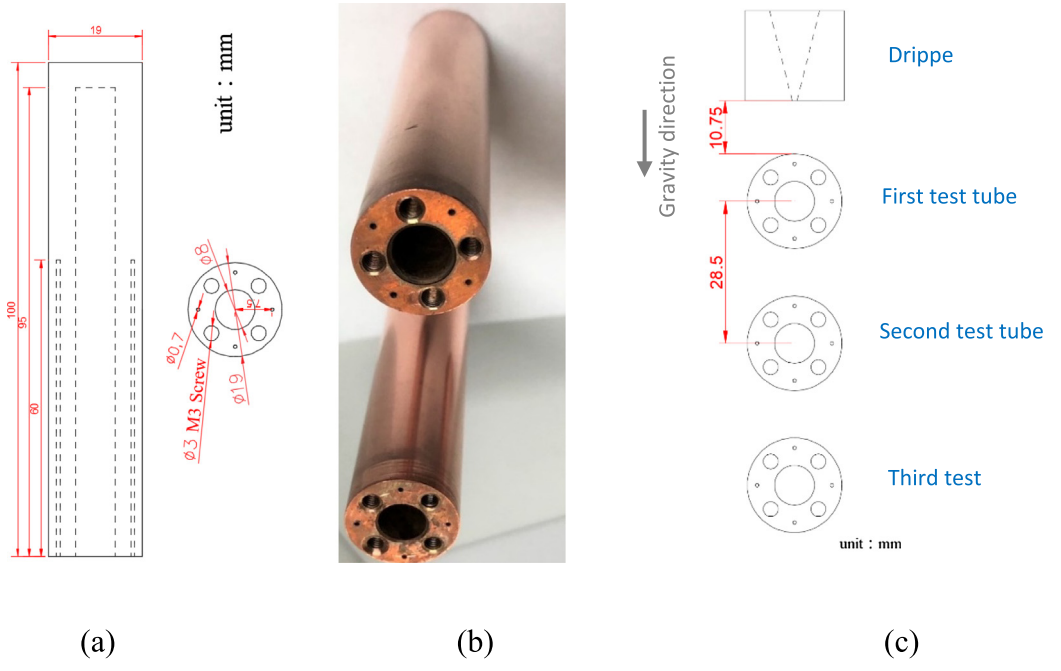

Fig. 3. The tubes of the experiment setup. (a) The details of the test tube drawing, (b) the actual photo of the machined test tube, (c) the details of test tube mounting and distances.

reworked with an inner diameter of 8 mm and a depth of 95 mm. A heater rod with the outer diameter of 7.6 mm and the total length of 95 mm is placed inside of each test tube. The active heating zone of the heater rod is 80 mm from its beginning, and hence, the 15 mm end of the rod is a non-heating zone. Therefore, the effective heating zone of the heater is L_H = 80 mm. In order to measure the wall temperature of each tube, four tiny thermocouples were utilized. In order to place the thermocouples and their wires inside the tubes, small holes of length 60 mm are machined by electric discharge in the test tubes as depicted in Fig. 3. The outer diameter of thermocouples holes was 0.7 mm and they placed with the distance of 7.5 mm from the center of the test tube in radial direction.

The test tubes are vertically arranged on the experimental support and locked with four M3 screws. In the present study, the top, middle and bottom test tubes are referred as test tubes 1, 2 and 3 respectively. The dripper feeder is locked with M5 screws above the test tubes. The spacing between the test tubes is fixed as 1.5-fold of the tube diameter, i.e. 28.5 mm. The dripper is mounted at the top of test tubes whereas the distance between the nozzle-tip of the dripper and the top of the test tube 1 is 10.75 mm.

Table 1
The experiments parameters.

Type	Value
Drip height (F_h)	10.75 mm
Drip pitch (W)	12 mm and 24 mm
Drip temperature (T_o)	20 °C
Dropper style (Feeder)	Stainless steel strip internal drilling into seven nozzles-holes in total, 4 holes each time
Drip flow of each nozzle-hole	50, 100 and 150 mLPM
Effective heating length (L_H)	80 mm
Heat flux (q)	5, 10, 15, and 20 kW/m^2
Test tube length (L_t)	100 mm
Test tube outer diameter (D)	19 mm
Test tube spacing	28.5 mm
Test tube style (type)	Smooth round tube
Working fluid	H_2O

3. Experimental procedure

The experiment is carried out by using different flow rates, heat generations and nozzles pitches. For each experiment, the flow

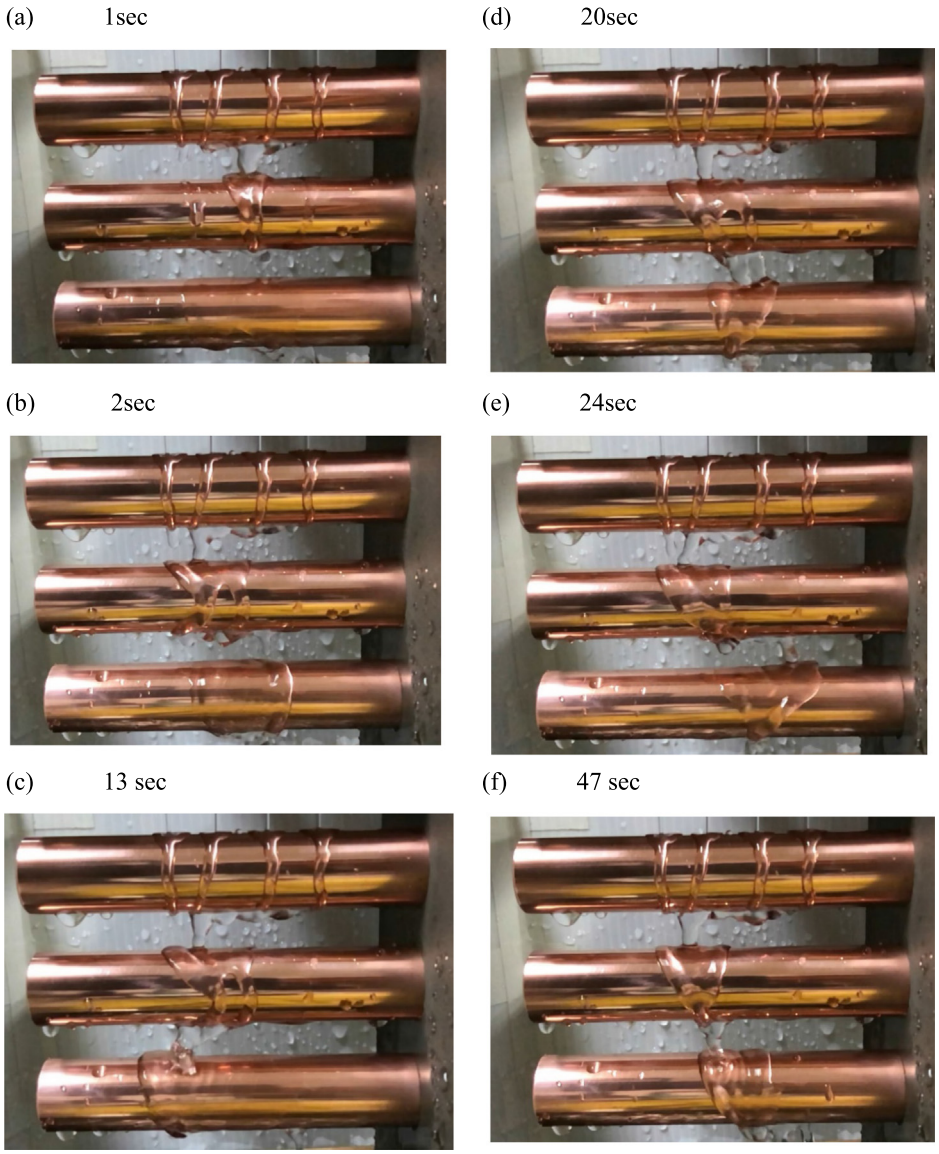

Fig. 4. The flow states for Case I when the flow rate of a single nozzle-hole is 50 mLPM. (a) t = 1 s, (b) t = 2 s, (c) t = 13 s, (d) t = 20 s, (e) t = 24 s, (f) t = 47 s.

field state under different conditions is observed. Table 1 shows the parameters of the experiments. As mentioned, in the feeder there are seven nozzles-holes. To examine the effect of the nozzles pitch in a constant flow rate, only four of the nozzles are utilize at a time in each experiment. The nozzles-holes of 2–5 were employed for the case of 12 mm pitch, i.e. Case I, and the nozzles-holes of 1, 3, 5 and 7 were employed for the case of 24 mm pitch, i.e. Case II. The flow rate of each nozzles-hole is measured by a beaker during one minute of time. An electronic weighting scale was also utilized as confirmation. The flow rates were adjusted by adjustable values to the flow rates of 50, 100 and 150 mLPM corresponding to the three specified flow rates of the experiments. The heat flux q is provided by a DC power supply that supplies DC power to the heating rod and then to the test tube. In this experiment, four heat fluxes of 5, 10, 15, and 20 kW/m^2 were tested.

3.1. Calculation of the results

The amount of the total heat generated in the rod (Q) can be evaluated using the measurement of the supplied voltage (V) and the current of the element (I) as $Q = V \times I$. The heated surface area (outer heated surface) of each test tube (A) can be simply calculated as $A = \pi \times D \times L_H$ where D is the outer diameter of the test tube and L_H is the effective heated length of the tube. Then, the heat flux (q) is evaluated by dividing the total amount of the generated heat (Q) by the heated surface area of the test tube as $q = Q/A$. The heat transfer coefficient (h) is calculated by dividing the heat flux (q) by the temperature difference (ΔT) as $h = q/\Delta T$ where ΔT is calculated as the difference between the average temperature of the tube wall (T_w) measured by the test tube quarter points minus the outlet temperature T_o of the drip hole nozzle, i.e. $\Delta T = T_w - T_o$.

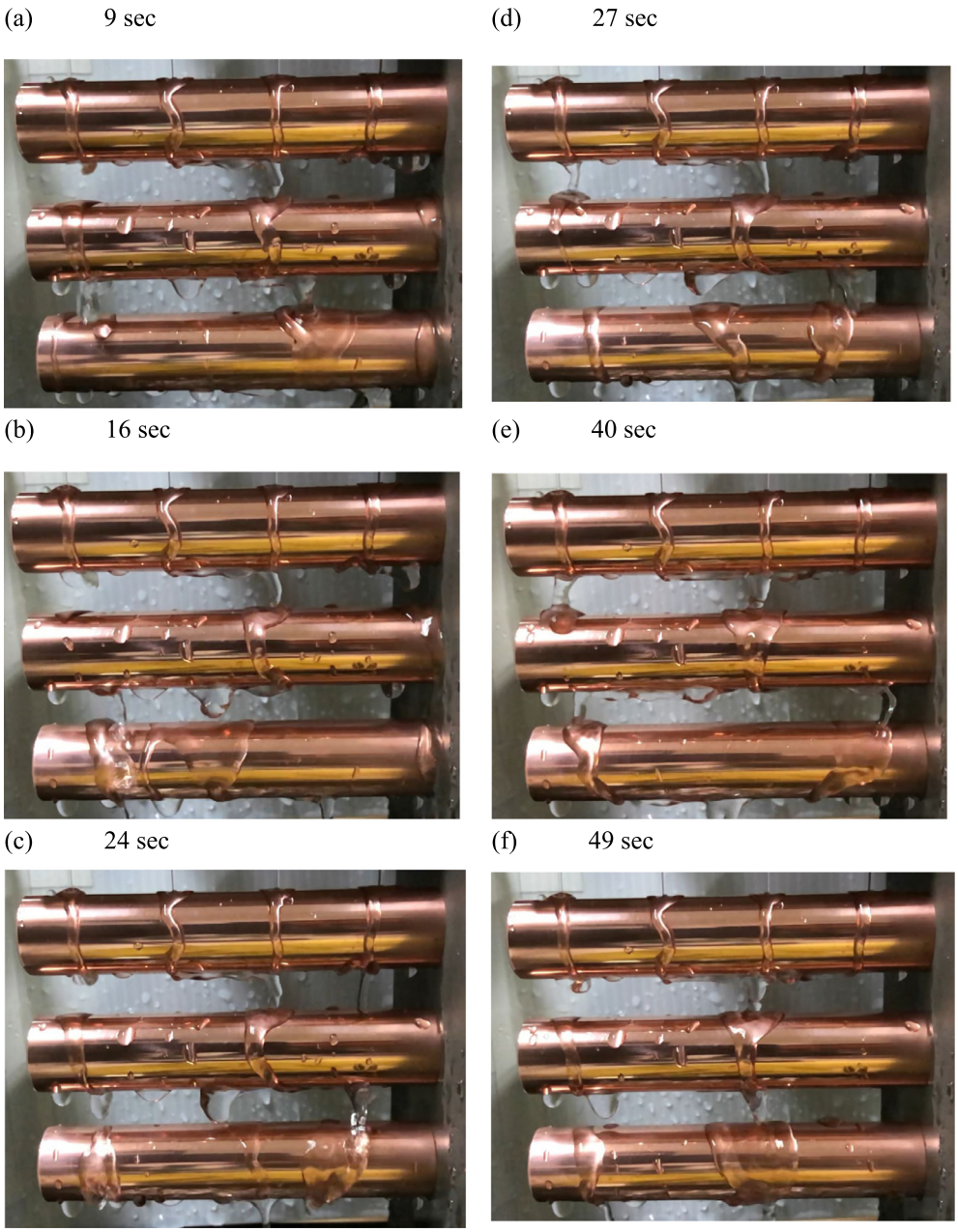

Fig. 5. The flow states for Case II when the flow rate of a single nozzle-hole is 50 mLPM. (a) t = 9 s, (b) t = 16 s, (c) t = 24 s, (d) t = 27 s, (e) t = 40 s, (f) t = 49 s.

3.2. The experiment instruments

The utilized isothermal bath (ALPHA RA 24; LAUDA) provides the accuracy of ±0.05 °C, and its cooling capacity is 0.425 kW at 20 °C. To support the required power of the heated rods mounted inside the test tubes three DC power units were utilized. Two of the power supply models are 62006p-100-25 and the manufacturer is Chroma. The third one is an APS-1102A and the manufacturer is Gwinstek. The utilized data acquisition system for temperature measurement is consist of a data acquisition unit (MX110-UNV-M10; Taiwan Yokogawa Co., Ltd) that is connected to the thermocouple wires and transmits the measured wall temperatures to a personal computer to calculate the heat transfer coefficient. The utilized thermocouples measuring the wall temperature of T_w are K-type with an accuracy of ±0.5 °C.

The system of time and beaker is utilized to measure the flow rate of each nozzle during one minute of discharging water. An electronic weighing scale is also utilized as a confirmation. A halogen light source (V501, Moritex and Affirmation Information Technology Co., Ltd) associated with a proceeding lens are employed for photographing the side of the flow over the tubes. A high-speed camera (CM3-U3-13Y3M) with the resolution of 1280 × 1024, the frame rate 124 FPS, and the pixel size 4.8 μm is used to capture the shapes of the water film over the test tube 1. Then, a computer software: IC Measure is employed to measure the thickness and other characteristics of the liquid film manually. After each test, the red copper test tubes were wiped with copper oil to remove the oxide layers and water marks, and they washed with alcohol and then with water and finally dried.

3.3. Experimental procedure

There are three main parameters in this experiment: (1) flow rate, (2) heat generation, and (3) drip pitch. The heat transfer performance is studied under different circumstances through different combinations of the main parameters. During the experiments, a high-speed camera captures the formation of the water film at the cross section of the test tube, and the camera on the side of the array photographs the film formation of the fluid on the array. The computer also recorded the temperatures.

4. Results and discussion

This section is divided into two parts: study of the flow field phenomenon and the study of the heat transfer performance. The flow field characteristics the flow phenomenon on the test tube arrays are examined using the side photo shots. The thickness of the liquid film at the test tube 1 with different flow rates and different drip pitches is also studied. In the second section, the wall temperatures and heat transfer performance are studied for various drip pitches, flow rates and surface heat flux powers.

4.1. Flow field phenomenon

This section mainly discusses the formation of liquid film at different flow rates and two cases of W = 12 mm (Case I) and double drop distance W = 24 mm (Case II). Figs. 4 and 5 illustrate the flow states for the Cases I and II, respectively when the flow rate of each of the nozzles-holes is 50 mLPM. Fig. 6(a) and (b) depict the steady liquid film thickness for Case I and Case II, respectively when the flow rate is 50 mLPM.

As seen in Fig. 4, the dripped water of each of the nozzles-holes has reached the uppermost tube (test tube 1) and formed four liquid films. During the initial times, the liquid films slightly extend to a certain distance and then bulge and then gather, and flow toward the bottom of the tube in the circumferential direction until they reach to the tube bottom where they fall over the test tube 2. The water films that dripped over the middle tube (test tube 2) form a liquid film over the test tube 2 with an irregular pattern that drifts to the left and right. After a certain period (usually within 50 s), it reaches to a stable state and only slightly sway.

As mentioned, Fig. 5 depicts the flow pattern photos for Case II. A comparison between the results of this figure and those depicted in Fig. 4, shows the similar general trend of flow pattern for the first test tube, i.e. test tube 1. In both cases, bulging and gathering, and flowing of the fluid films and movement toward the bottom of the tube in the circumferential direction can be observed. However, the results for the second and third tube tests are different. For Case I, which the nozzles-holes are closer to each other, the water flow merges over the second tube and results in a wide film moving in the circumferential direction. When the film falls over the third tube (test tube 3), it also forms a wide film in the circum-

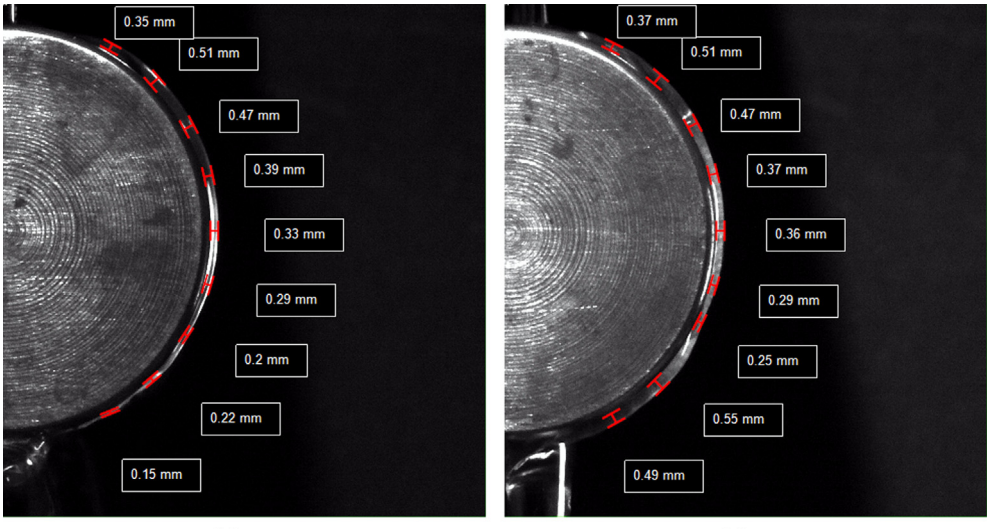

(a) (b)

Fig. 6. The liquid film thickness (δ) over the test tube 1 when the flow rate of a single nozzle-hole is 50 mLPM. (a) Case I, (b) Case II.

ferential direction, and then falls into the bottom of the test section to be accumulated and circle back.

In Case II, in which the distance between the nozzles-holes is large, the falling films, which reach the second tube form two wide films. These two films also fall over the third tube and form almost the same film pattern as the second tube and finally fall into the bottom of the test section. Fig. 6(a) shows almost similar thickness patterns for both Cases of I and II. The thickness of the liquid film increases from 30° to 75°, and then, it decreases from 75° to 150°. The increase in the film thickness is because of the film shrinkage. The increase of the film thickness is due to the acceleration of the fluid in downward direction and consequently the increase of liquid velocity.

The flow patterns for Cases I and II are depicted in Figs. 7 and 8, respectively when the flow rate for each nozzle-hole is 100 mLPM. Fig. 9(a) and (b) illustrate the steady thickness of the liquid film over the test tube 1 for Case I and Case II, respectively when the flow rate is 100 mLPM. A comparison between the flow patterns of Figs. 7 and 4 shows that the increase of the flow rate of each nozzle-hole has induced a significant effect on the flow patterns. Here in Fig. 7, it is clear that the increase of the flow rate increases the amount of the liquid that reaches to the first tube. The drops of nozzles merge in the top section of the test tube 1 and form a wide film there. The reason for this bonding can be the fact that the sufficient flow rate of water has smoothly reaches the top section of the test tube where the velocity of the drip reaches to zero immediately after touching the top surface of the test tube. The liquid with zero velocity forms a thick film there. As the film of liquid is thick, it tends to flow in both of the axial and angular directions. The flow in the axial direction results in the increase of the film width. As the nozzles-holes in the case 1 are close to each other, the liquid easily reaches to its neighbor film, and hence, the neighbor films merge into one film. Then, the liquid film accelerates in the angular direction and moves downward over the circumference direction of the tube.

Following the flow behavior in time sequences, Fig. 7 demonstrates that the liquid film bonds after stretching and produces a large wet area over the test tube 1. This bond is almost stable after

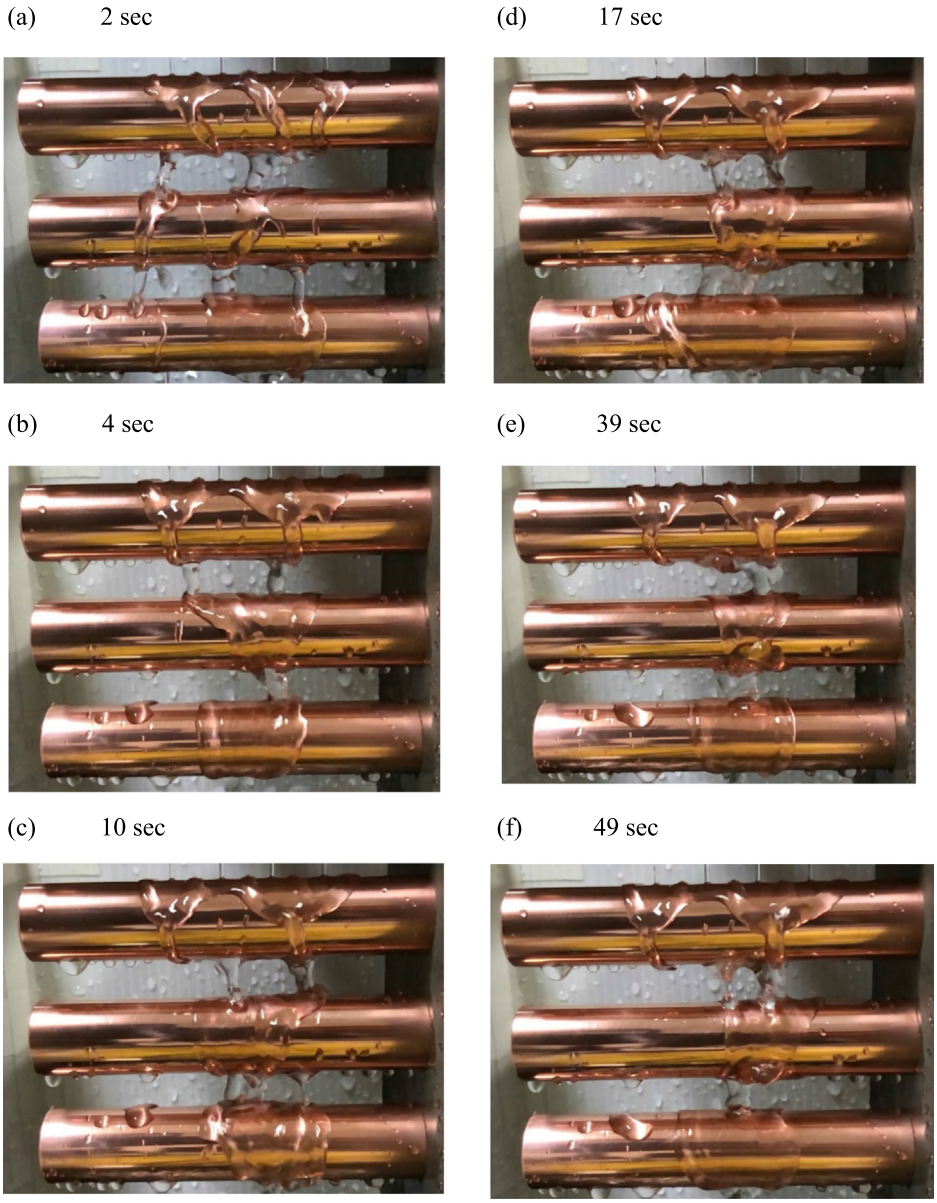

Fig. 7. The flow states for Case I when the flow rate of a single hole is 100 mLPM. (a) t = 2 s, (b) t = 4 s, (c) t = 10 s, (d) t = 17 s, (e) t = 39 s, (f) t = 49 s.

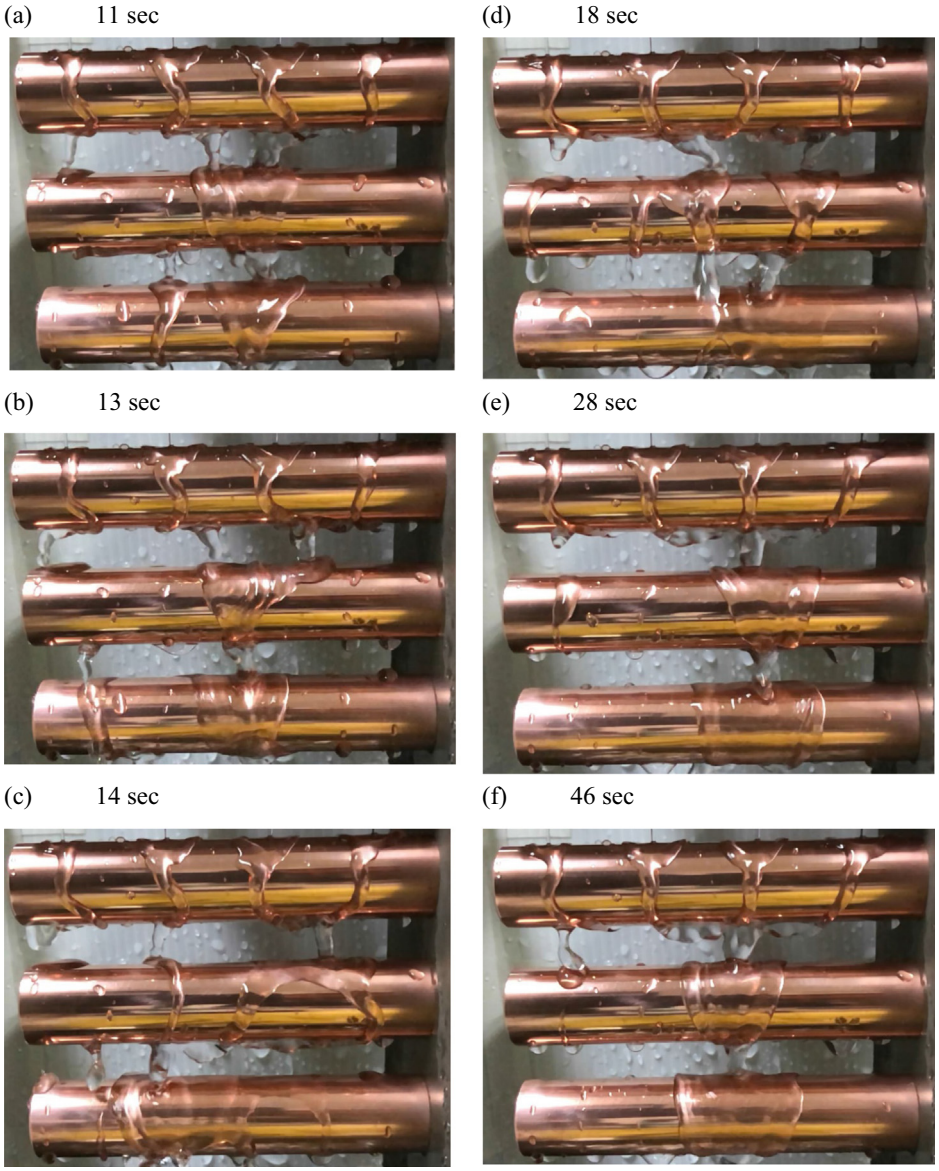

Fig. 8. The flow states for the Case II when the flow rate of a single hole is 100 mLPM. (a) t = 11 s, (b) t = 13 s, (c) t = 14 s, (d) t = 18 s, (e) t = 28 s, (f) t = 46 s.

39 s where the liquid completely saturated the top section of the first tube. As the liquid film moves in angular direction toward the bottom of the tube, the angular velocity of the liquid increases. The increase of the liquid velocity results in the decrease of the film thickness due to the continuity of the liquid. The decrease of the film thickness can be observed in Fig. 9(a) where the thickness of the film decreases from 18 mm at the most top section about 30° from top of the tube to 0.1 mm at about 45°. Then the films get unstable and tend to shrink and reduce the film width, which it results in the increase of film thickness. This behavior continues from 60° with 0.16 mm film thickness until 120° where the highest thickness of the film with 0.65 mm can be observed. After this the liquid further accelerates and results in the further increase of the liquid velocity. Fig. 7(f) shows that the width of the liquid film is almost constant after 120°. Hence, the increase of the liquid velocity after 120° results in the decrease of the film thickness due to the continuity of the fluid. In this case the film thickness decreased from 0.65 mm at 120° to 0.35 mm at 150°. After this, the liquid film again goes into an unstable condition and forms a thick film and falls over the test tube 2.

Fig. 8 shows the flow patterns in different time sequences for Case II with 100 mLPM flow rate of at each nozzle hole. As seen, the drops over the top section of the tube test 1 forms four separate films. The films are wide at the top of the tube. However, as the distance between nozzles-holes is doubled the extended width of the films over the top section of the tube is not enough to bond the films. In this case, the flow pattern and its behavior is almost similar to Case I with lower flow rate of 50 mLPM. In this figure also it can be seen that during the initial times the liquid films slightly extend to a certain distance and then bulge and then gather, and flow to the bottom of the tube in the circumferential direction until they reach to the bottom of the tube where they fall over the bottom test tube. Here, the difference is that the three of the falling films drops, which come from nozzles-holes of 1, 3, and 5, have merged at the bottom of the tube and then drip together over the second tube. The nozzle 7 almost works separately, but as seen in Fig. 4, all of the falling films merge and then fall over the test tube 2.

Attention to Figs. 8(f) and 9(b) shows that as the liquid film starts to shrink at 30°, its thickness significantly increases from

0.19 mm at 30° to 0.49 mm at 45°. Then, the liquid film starts to sway around the periphery of the horizontal tube from 60° to 135°, and the thickness of the film fluctuates smoothly abound 0.61 mm. After 135°, the film thickness reduces from 0.63 mm at 135° to 0.48 mm at 150° due to the further increase of the liquid velocity in circumferential direction. Then, it goes to a new form to be collected at the bottom of the tube and falls over the test tube 2. Attention to Fig. 8 also depicts that the drops of test tube 2 form a large falling film and a small falling film over test tube 3. The large falling film is the result of the drops of the first three nozzles, i.e. 1, 3 and 5, that merged and almost covered the middle section of the test tubes of 2 and 3. The small drop is the result of the last separated film of nozzle 7. These trends of the results are in agreement with those reported in the study of Qiu et al. [9].

The flow patterns for Cases I and II are depicted in Figs. 10 and 11, respectively when the flow rate for each nozzle-hole is 150 mLPM. Fig. 12 shows the steady film thickness over the test tube 1. Fig. 10 shows that the liquid film extends in a longer distance and surrounds the test tube 1 with a wider layer, and hence, all of the drops corresponding to the four nozzles are bonded to a sin-

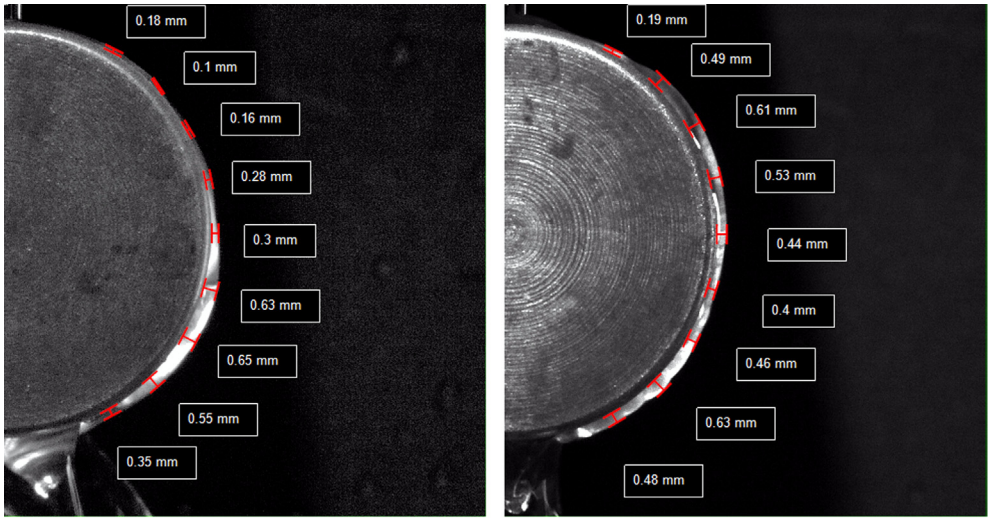

Fig. 9. The liquid film thickness (δ) over the first test tube when the flow rate of each nozzle-hole is 100 mLPM. (a) Case I, (b) Case II.

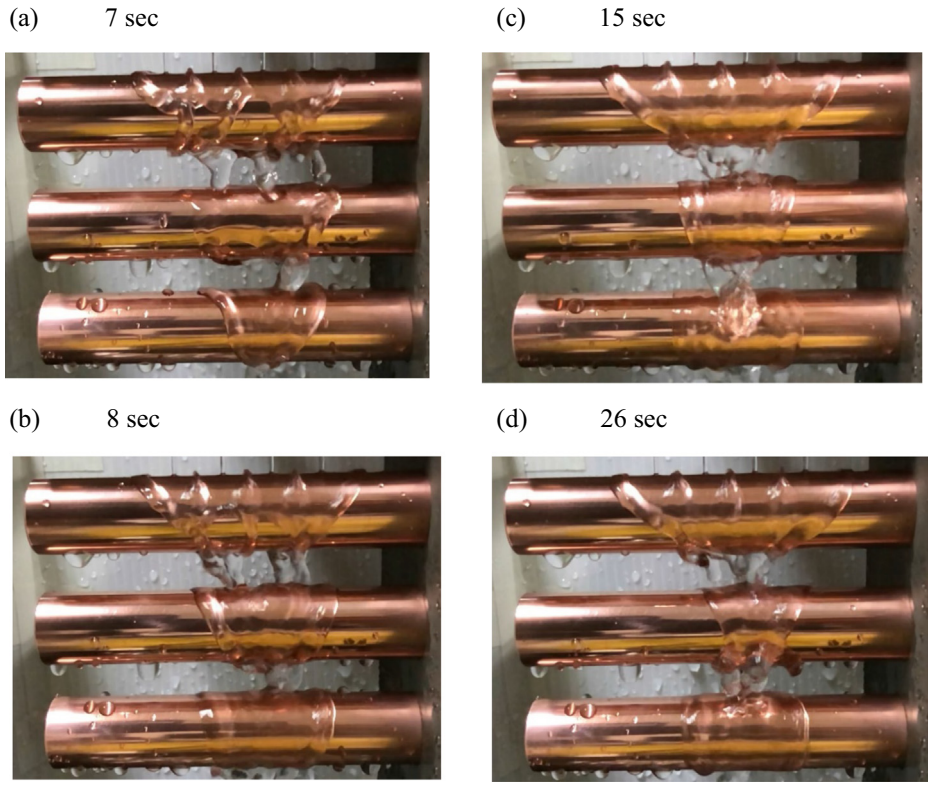

Fig. 10. The flow states for the Case I when the flow rate of a single hole is 150 mLPM. (a) t = 7 s, (b) t = 8 s, (c) t = 14 s, (d) t = 18 s.

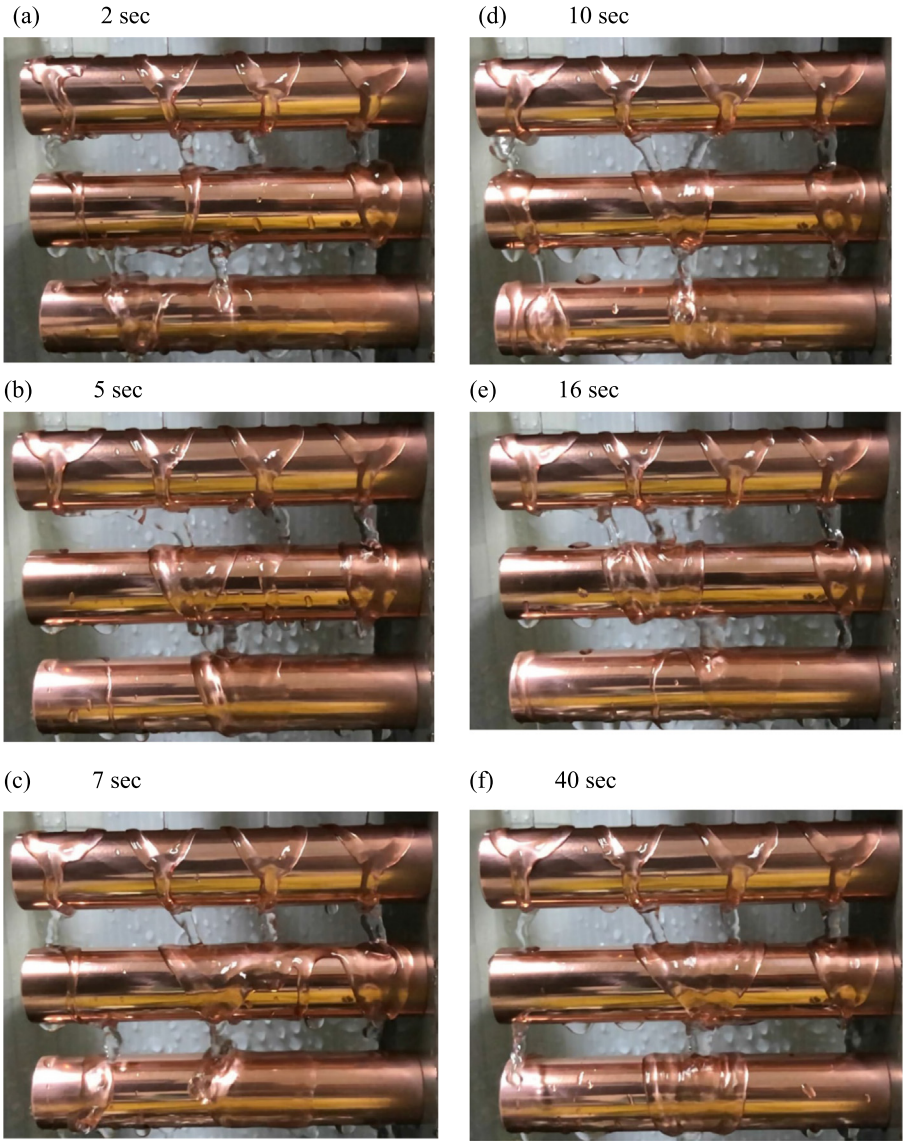

Fig. 11. The flow states for the Case II when the flow rate of a single hole is 150 mLPM. (a) t = 2 s, (b) t = 5 s, (c) t = 7 s, (d) t = 10 s, (e) t = 16 s, (f) t = 40 s.

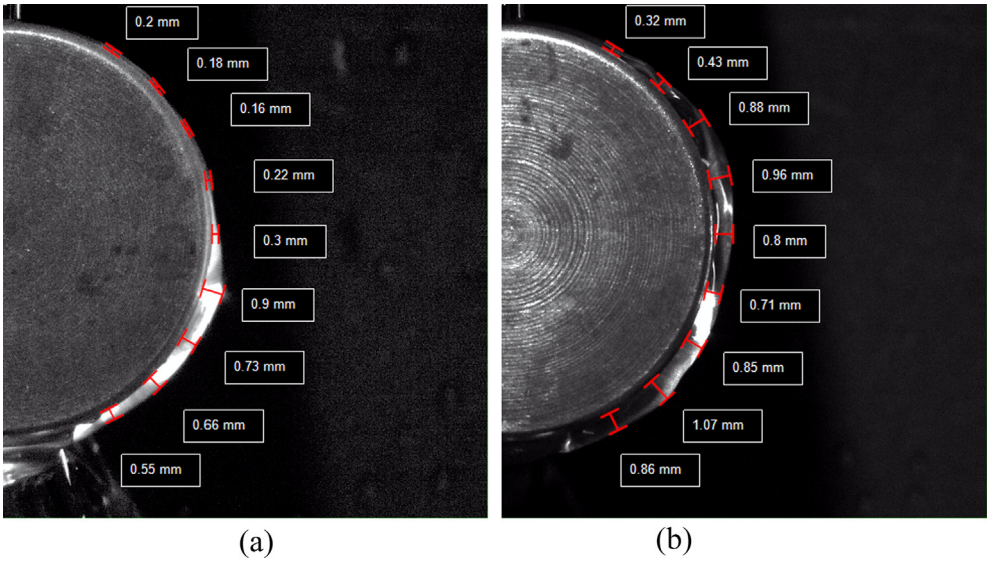

Fig. 12. The liquid film thickness (δ) over the first test tube when the flow rate of a single nozzle-hole is 150 mLPM. (a) Case I, (b) Case II.

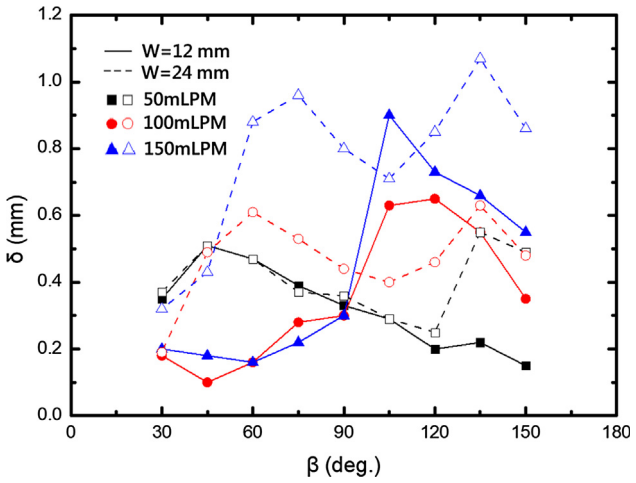

Fig. 13. liquid film thickness (δ) at different flow rates and two Cases I (W = 12 mm) and II (W = 24 mm).

gle and wide liquid film. So that, the upper tube is completely covered by the liquid film just below the nozzles-holes. Time sequence photos of Fig. 10 illustrate that Case I is stabilized in a matter of seconds.

As seen in Fig. 11, the significant extension of the liquid film over the top section of the test tube 1 is not enough to join the films of nozzles in Case II, which the distance of the nozzles-holes is large. Hence, four separated Y-shaped films are formed over the test tube 1. Fig. 11(f) depicts that the drops of two middle nozzles of 3 and 5 merged and dropped over the test tube 2 where they almost covered the middle section of test tube 2. The film of nozzles 1 and 7 is also separately falls over test tube 2. The shrinking areas over test tube 2 are extremely small. The flow pattern of the test tube 2 is almost repeated over test tube 3, i.e. a large drip, which is the combine of two nozzles at the middle and two separate films at the sides.

Attention to the results of the film thickness for Case I in Fig. 12 (a) demonstrates that the thickness of the liquid film starts to decrease monotonically from 0.2 mm at 30° to 0.16 mm at 60°. This

Table 2
The measured wall temperatures of the test tubes in one drop interval.

q (kW/m^2)	Flow rate (mLPM)	Sensor position	Case I			Case II		
			Test tube 1	Test tube 2	Test tube 3	Test tube 1	Test tube 2	Test tube 3
5	50	0°	25.1	29.4	31.9	25.2	28.8	30.6
		90°	25.5	28.9	32.2	25.4	28.3	30.9
		180°	25.3	28.8	31.9	25.2	28.1	30.5
		270°	25.3	29.0	32.1	25.2	28.6	30.8
	100	0°	22.9	24.5	26.8	23.3	26.5	27.9
		90°	23.3	24.6	27.1	23.6	26.2	28.2
		180°	23.2	24.5	26.8	23.4	25.8	27.8
		270°	23.1	24.6	27.1	23.4	26.3	28.1
	150	0°	21.9	23.5	24.0	22.0	23.0	24.5
		90°	22.3	23.3	24.3	22.3	23.1	24.7
		180°	22.2	23.3	24.2	22.2	23.1	24.7
		270°	22.0	23.4	24.5	22.0	23.1	25.0
10	50	0°	27.6	35.5	40.0	28.0	34.9	38.5
		90°	28.3	34.8	40.4	28.4	34.0	38.8
		180°	28.1	34.8	40.1	28.2	33.8	38.5
		270°	28.0	35.0	40.6	28.3	34.6	38.7
	100	0°	24.3	27.1	28.5	24.7	28.5	30.3
		90°	25.0	27.4	28.9	25.3	28.4	30.7
		180°	25.1	27.2	28.8	25.1	28.5	30.5
		270°	24.8	27.3	29.0	25.1	28.7	30.9
	150	0°	22.9	25.9	26.9	22.8	24.9	26.7
		90°	23.6	25.7	27.4	23.3	25.1	27.2
		180°	23.6	25.8	27.3	23.3	25.2	27.2
		270°	23.4	25.9	27.6	23.1	25.2	27.5
15	50	0°	30.4	42.1	48.4	30.8	40.4	46.2
		90°	31.3	41.0	48.9	31.4	39.4	46.7
		180°	31.1	41.2	48.7	31.1	39.2	46.3
		270°	31.1	41.4	48.5	31.2	40.3	46.3
	100	0°	25.5	29.6	31.1	26.2	30.8	33.4
		90°	26.4	30.1	31.8	26.9	31.0	34.0
		180°	26.7	29.9	31.8	26.8	31.4	34.2
		270°	26.3	29.9	32.0	26.6	31.4	34.3
	150	0°	24.0	28.3	29.7	23.6	26.4	29.3
		90°	24.9	28.1	30.4	24.3	26.6	29.9
		180°	25.1	28.2	30.5	24.4	26.8	30.1
		270°	24.7	28.3	30.6	24.1	26.8	30.3
20	50	0°	33.0	48.4	56.7	33.7	47.2	53.9
		90°	34.2	47.0	57.4	34.4	45.9	54.6
		180°	33.9	47.2	57.1	34.1	45.8	54.3
		270°	33.9	47.4	56.8	34.2	47.3	54.2
	100	0°	26.9	32.7	34.3	27.7	34.2	35.9
		90°	28.2	33.3	34.7	28.7	34.5	36.8
		180°	28.5	33.1	34.7	28.7	35.5	37.0
		270°	28.0	33.2	35.0	28.4	35.2	36.9
	150	0°	24.6	29.9	32.0	24.6	29.0	30.3
		90°	25.8	29.9	32.7	25.3	29.2	31.0
		180°	26.0	30.3	33.0	25.5	29.8	31.4
		270°	25.6	30.3	33.1	25.2	29.5	31.5

is due to the fact that the flow rate is high and the thickness of the flow film is enough to remain wide, and hence, the film does not enter the shrinking state. After that, the film thickness starts to increase smoothly until 90° due to the smooth shrinking behavior of the film. Then, a sudden sharp increase in the film thickness can be observed at 105°, which is the result of a significant film shrinkage. After that, the decrease of the film thickness occurs due to the increase of the liquid film velocity. Fig. 12(b) depicts the behavior of the film thickness for Case II. In this case, the initial film thickness at 30° is 0.32 mm is larger than the thickness of Case I with the same position and flow rate, i.e. 0.2. This is because the films of the nozzles does not merge at the top section of the test tube 1, and hence, it covers a smaller area over the tube. In the Case I, it is was observed that the thickness of the liquid film decreases by the increase of the angle from 30° to 60°. However, in the Case II, the thickness of the film increases by the increase of angle from 30° to 75°. The reason for this increase is the formation of Y-shaped films in this area. After the angle of 75°, the liquid film starts so sway over the tube surface, and as a result, the liquid film thickness smoothly fluctuates.

Fig. 13 shows the steady thickness of liquid film (δ) over the test tube 1 as a function of angle of the tube (β) for various flow rates and the two studied Cases I and II. The angle of β is measured from the top of the tube in clockwise direction. The solid lines with filled symbols represent the film thickness (δ) of Case I, i.e. $W = 12$ mm, and the dotted lines with the hollow symbols represent δ of Case I, i.e. $W = 24$ mm. The flow behavior and the thickness of the liquid film was discussed in previous figures. Here, Fig. 13 indeed shows a summary of the thickness behavior of the liquid films in studied experiments. This figure shows that the trend of the behavior of the three flow patterns of 50, 100 and 150 mLPM for Case II are the same. The liquid thickness first increases to angles about 45–60°, then it starts a decreasing trend until angles about 105–120°. Then, the thickness of the liquid film starts an increasing trend of behavior to reach angles about 135°. Finally, a sharp decrease of thickness at 150° occurs. The increase in the thickness of the liquid film at the small angles about 45–60° is due to the shrinking of the liquid film. The decrease and then the increase of the thickness in angles about 60–135° are due to the gravity effect and aggregation. This similar trend of behavior for Case II is due the fact that the distance between the nozzles-holes is large and the liquid film of a nozzle cannot form a bond between its neighbor liquid films, induced by the neighbor nozzles.

In Case I and flow rates of 100 and 150 mLPM, the thickness of the liquid film first decreases (about 60°) and then increases (up to 105°) and finally decreases (up to 150°). The decrease of δ at the small angles (about 60°) is due to the bonding of liquid films. The observed increase of δ in the interval of $\beta = 60$–$105°$ is due to the shrinking of the liquid film. Finally, the observed reduction of δ for large value of β is due to the gravity effects.

Study of the thickness behavior of the liquid film for Case I shows that the trend of behavior of the low flow rate of 50 mLPM is different of the other cases of 100 and 150 mLPM. It almost follows the trend of the results of Case II until 90°. After 90°, in contrast with Case II, which shows an increasing trend of thickness, the liquid thickness still shows a decreasing behavior. As the flow

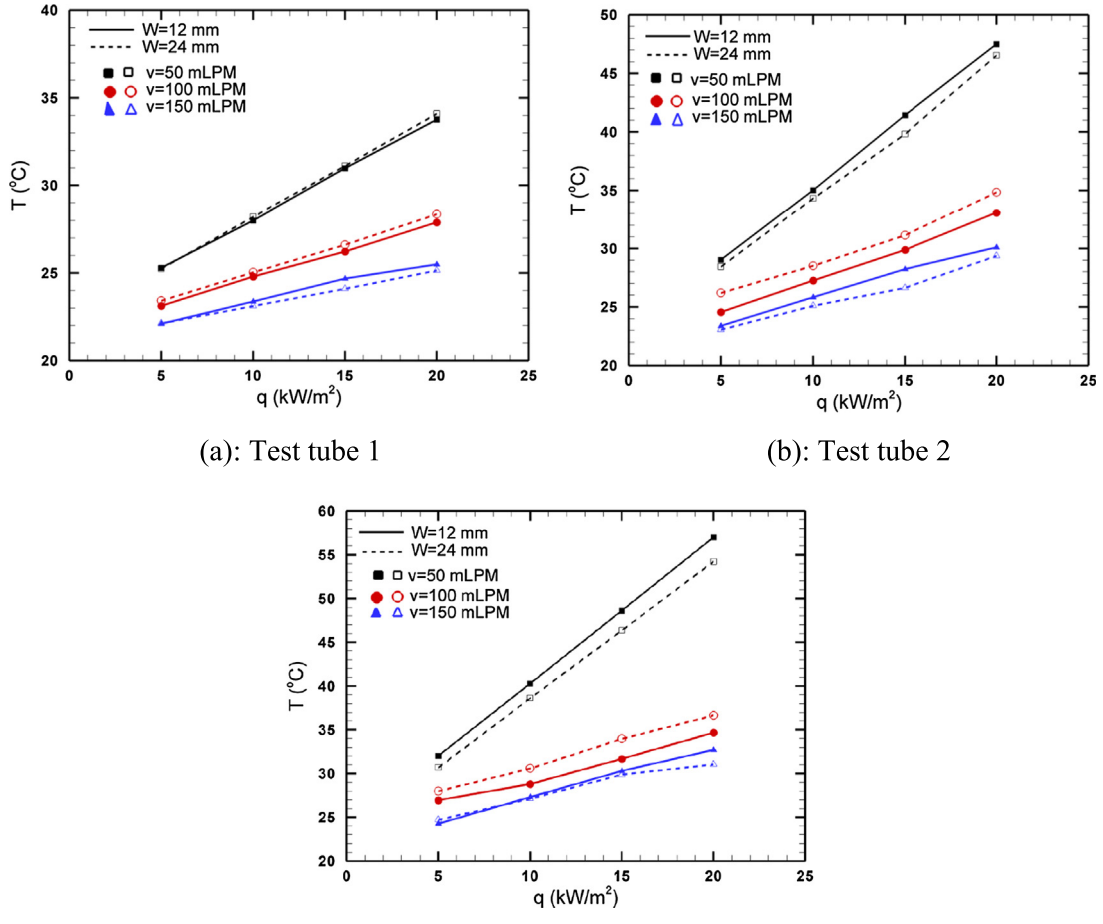

Fig. 14. The tube wall temperature as a function of tube heat flux for various volume rates for (a) test tube 1; (b) test tube 2 and (c) test tube 3.

rate of 50 mLPM is very low, the liquid film over the top of the test tube 1 extends in a small area, and hence, it does not bond with its neighbor liquid films (the same as the Case II). However, as it was observed in Fig. 4, at the bottom of the tube, the liquid films make a bond in the middle of the test tube 1 and then fall over the test tube 2.

4.2. Heat transfer performance

The important parameter for calculating the heat transfer coefficient is the tube wall temperature. The wall temperature of each of the test tubes is measured in four points at $\beta = 0°$, 90°, 180° and 270° where β is evaluated from the top of the test tube in clockwise direction. The measured temperatures are summarized and reported in Table 2 for various tube heat flux rate (q), various flow rates and for two nozzle arrangements of Cases I and II. The results of Table 2 indicate that the temperature fluctuation of each test tube is very low about 1 °C for each experiment. This table also shows that the increase of the flow rate always reduces the wall temperatures of the test tubes. The temperature of the test tube 1 is almost the same for both nozzles arrangement of Cases of I and II. However, the change of the nozzles configuration notably changes the temperature of the test tubes 2 and 3. The measured temperatures of Table 2 were also utilized for calculating the convective heat transfer coefficient of h over the tube walls. The results of this table also of interest for validation of future numerical results.

The liquid film absorbs the heat of the test tubes via the convective heat transfer mechanism. The formation and flow of the liquid film directly affect the temperature of the measuring points. The four measured steady temperatures at the wall of each test tube can be converted to convective heat transfer coefficient using the equation of $h = q/\Delta T$ which was introduced in Section 3.3.

Fig. 14 shows the average surface temperature of each test tube as a function of heat flux. In Fig. 14, the test tube 1, 2 or 3 stands for the test tube located at the top, middle, or bottom, respectively. As seen, the increase of heat flux increases the tube temperature for all of tubes. It is also clear that the increase of the flow rate decreases the temperature of tubes. It is found that when the flow rate is low (50 mLPM), using Case I (W = 12 mm nozzles configuration distance) results in smoothly lower temperature in test tube 1 (in comparison with that of Case II (W = 24 mm), but it increases the temperature of tubes 2 and 3. When the flow rate increases to 100 mLPM, Case I shows a significant drop in all of the tubes temperatures compared to the Case II. By further increase of the flow rate to 150 mLPM, the temperature of Tubes 1 and 2 for Case I is higher than that of Case II. This is because of the type of the formation of the liquid film over the tubes, which was discussed in previous figures.

Fig. 15 illustrates the convective heat transfer as a function of flow rate for various values of heat flux (q). This figure demonstrates that the increase of the flow rate always enhances h. This finding was also clear in the results of Table 2 where the increase of the flow rate always reduces the temperature of the tubes. Fig. 15 also shows that the increase of heat flux increases the convective heat transfer coefficient of h in most cases. This figure also indicates that the nozzles configuration of Case II usually results in better heat transfer coefficient of h.

From comparison of Fig. 15(a)–(d) it can be observed that the change of the nozzles configuration in Cases I and II smoothly

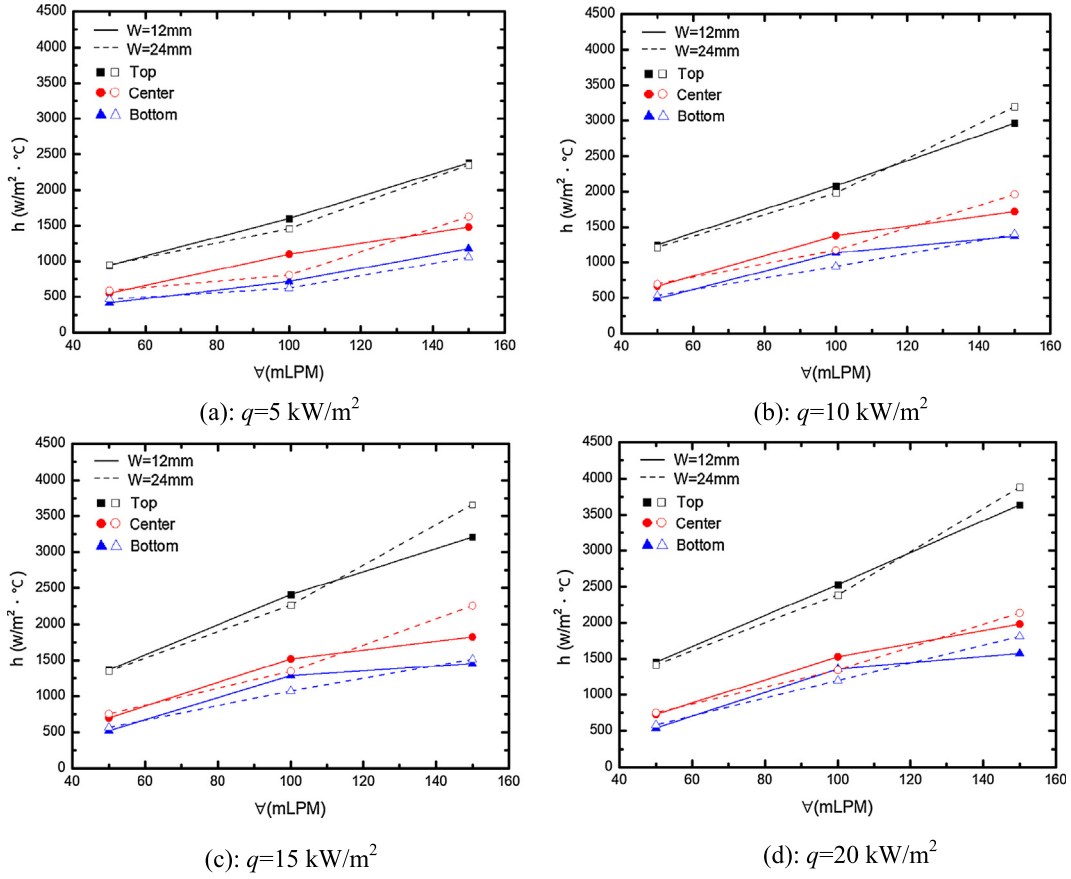

Fig. 15. Comparison of convective heat transfer coefficient of test tubes at various heat fluxes as a function of volume rate, (a) q = 5 kW/m^2; (b) q = 10 kW/m^2; (c) q = 15 kW/m^2; (d) q = 20 kW/m^2.

affects the convective heat transfer coefficient of h when the flow rate is low, i.e. 50mLPM. Fig. 14 also depicts that the convective heat transfer coefficient (h) for the test tube 1 is almost twice of h for the test tubes 2 and 3. It is also clear that the configuration of the nozzles also does not induce a notable change of h for the test tubes 2 and 3. This is because of the flow behavior of the steady liquid film, which was observed in Figs. 4(f) and 5(f). In both Cases I and II, there were four separate liquid films, which each of them smoothly extended over the top of the first tube. However, in contrast to Case II, in which the liquid films do not bond at the bottom of test tube 1, in this case, the liquid films bond at the bottom of the test tube 1 and form one or two falling films of water over the test tubes 2 and 3. These drops only cover a small portion of the test tubes 2 and 3, and hence, h for these test tubes is notably smaller than that of the test tube 1. The difference between h for test tubes 2 and 3 gets notable when the flow rate is high, i.e. 100 and 150 mLPM. The convective heat transfer coefficient of the test tube 2 (h) is almost twice of h for the test tube 3.

5. Conclusion

The flow behavior, film thickness of liquid film and the thermal performance of a falling water over horizontal tubes are studied experimentally. The main studied parameters were the flow rate, the tube heat flux, and the distance between the nozzles-holes. The flow behavior and film thickness were measured using cameras, and the wall temperatures were measured using the thermocouples embedded in the tube walls. The results were reported in the form of images, table of temperature and plots of the temperatures and convective heat transfer coefficient (h). The main outcomes can be summarized as follow:

1. The observed flow behavior can be divided into formation of a liquid film over a tube, the expansion of the film, the bonding of films, shrinking of a liquid film, and collection of the liquid at the bottom of a tube. The combination of these main behaviors may be occur depending on different parameters such as the flow rate and distance between the nozzles-holes. The behavior of the liquid film directly affects the heat transfer rate over the tubes.
2. When the water leaves the nozzles and reach to the top surface of the test tube 1, it moves in axial and circumferential directions and forms a film of liquid. The flow movement in the axial direction extends the film over the top of the tube and increases the width of the liquid film. It is found that the increase of the flow rate increases the width of the liquid film over the test tube 1. Depending on the expanding width of the liquid film and the distance between the nozzles-holes, the liquid films may bond or remain separate. In the case of bonded liquid films, the liquid film is very thin before 90°, and then its thickness rises sharply. If the liquid films do not affect each other after extending from the drop center (no bonding effect), the film thickness increases first, and then, decreases, and finally, it rises again.
3. In all of the studied experiments, it was found that the heat transfer coefficient (h) at the first test tube at the top (the test tube 1) is the highest, the test tube 2 in the middle is the second, and the test tube 3 at the bottom is the lowest. The larger the flow rate, the larger the heat transfer coefficient. The increase of the heat flux increases the convective heat transfer coefficient.
4. In the case of low flow rate of 50 mLPM, it was found that the convective heat transfer coefficient (h) for the test tube 1 is almost twice of the test tubes 2 and 3. It is also revealed that the configuration of the nozzles also does not induce a notable change of h for the test tubes 2 and 3. In the case of low flow rate and low heat flux, there is no significant difference in the heat transfer coefficient between the Case I (single nozzles spacing) and Case II (double nozzles spacing).
5. The difference between h for test tubes 2 and 3 gets notable when the flow rate is high, i.e. 100 and 150 mLPM. The convective heat transfer coefficient of the test tube 2 is almost twice of the convective coefficient of the test tube 3.
6. When the flow rate is high, i.e. 150 mLPM, and the heat flux is also high, i.e. 20 kW/m^2, the highest heat transfer coefficient is obtained in the Case II. The heat transfer coefficient h over the test tube 1 in Case I and Case II reaches to 3636 W/m^2°C and 3883 W. /m^2°C, respectively.

The results of the present study reveal that the nozzles distance is an important key parameter, which can control the liquid film bonding and heat transfer performance of the test tubes. It was observed that the bonding of liquid films, which is the result of the liquid film extension over the top section of the test tube, directly affects the fluid behavior of the falling film. Hence, special focus on the film extension over the top of a tube and its effect on the heat transfer is of interest that can be subject of future studies.

In the present study, the test tubes have been cleaned after each test to obtain uniform results. However, in practice and especially in evaporative applications, the walls surfaces of the tubes are under the influence of the working fluid and sediments. Hence, the systematic analysis of the effect of the sediments and the wall cleaning treatments is an important issue in long service application of these tube bundles, which can be the subject of future studies.

Another important point is that the falling film heat exchangers are usually employed in evaporation process; hence, study of falling film with evaporation for refrigerants as the working fluid is very important that it can be subject of future works. However, it is worth noting that experimenting with refrigerants, requires essential modifications in the present experimental setup such as proper sealing of the experiment chamber, adding a condenser and a compressor for recirculating the refrigerant.

Conflict of interest

The authors declared that there is no conflict of interest.

Acknowledgements

The authors appreciates the financial support from Ministry of Science and Technology, Taiwan, under grant number MOST 106-2221-E-027 -102 -MY2 and MOST 107-3113-E-027-001-CC2. The authors also appreciate the financially supported by the "Research Center of Energy Conservation for New Generation of Residential, Commercial, and Industrial Sectors" from The Featured Areas Research Center Program within the framework of the Higher Education Sprout Project by the Ministry of Education (MOE) in Taiwan.

References

[1] I.A. Hassan, A. Sadikin, N. Mat Isa, The computational modeling of falling film thickness flowing over evaporator tubes, J. Adv. Res. Fluid Mech. Therm. Sci. 14 (1) (2015) 24–37.
[2] G. Ribatski, A.M. Jacobi, Falling-film evaporation on horizontal tubes-a critical review, Int. J. Refrig. 28 (5) (2005) 635–653.
[3] V. Subramaniam, S. Garimell, Numerical study of heat and mass transfer in lithium bromide-water falling films and droplets, Int. J. Refrig. 40 (2014) 211–226.
[4] Y. Fujita, M. Tsutsui, Evaporation heat transfer of falling films on horizontal tube-Part 2: Experimental study, Heat Transf.-Jpn. Res. 24 (1) (1995) 42–55.

[5] R. Armbruster, J. Mitrovic, Evaporative cooling of a falling water film on horizontal tubes, Exp. Therm Fluid Sci. 18 (3) (1998) 183–194.
[6] F.A. Jafar, G.R. Thorpe, Ö.F. Turan, Falling film transition and heat transfer on horizontal circular cylinders, in: 17th Australasian Fluid Mechanics Conference, Auckland, New Zealand, 2010, pp. 5–9.
[7] F. Sun, S. Xu, Y. Gao, Numerical simulation of liquid falling film on horizontal circular tubes, Front. Chem. Sci. Eng. 6 (3) (2012) 322–328.
[8] H. Hou, Q. Bi, H. Ma, G. Wu, Distribution characteristics of falling film thickness around a horizontal tube, Desalination 285 (2012) 393–398.
[9] Q.G. Qiu, W.G. Jiang, S.Q. Shen, X.J. Zhu, X.S. Mu, Numerical investigation on characteristics of falling film in horizontal tube falling film evaporator, Desalin. Water Treat. 55 (2014) 3247–3252.
[10] X. Chen, S. Shen, Y. Wang, J. Chen, J. Zhang, Measurement on falling film thickness distribution around horizontal tube with laser-induced fluorescence technology, Int. J. Heat Mass Transf. 89 (2015) 707–713.
[11] M. Li, Y. Lua, S. Zhang, Y. Xiao, A numerical study of effects of counter-current gas flow rate on local hydrodynamic characteristics of falling films over horizontal tubes, Desalination 383 (2016) 68–80.
[12] J. Chen, R. Zhang, R. Niu, Numerical simulation of horizontal tube bundle falling film flow pattern transformation, Renewable Energy 73 (2015) 62–68.
[13] Q. Qiu, C. Meng, S. Quan, W. Wang, 3-D simulation of flow behaviour and film distribution outside a horizontal tube, Int. J. Heat Mass Transf. 107 (2017) 1028–1034.
[14] H. Hou, Q. Bi, X. Zhang, Numerical simulation and performance analysis of horizontal-tube falling-film evaporators in seawater desalination, Int. Commun. Heat Mass Transf. 39 (1) (2012) 46–51.
[15] C.Y. Zhao, W.T. Ji, P.H. Jin, Y.J. Zhong, W.Q. Tao, Hydrodynamic behaviors of the falling film flow on a horizontal tube and construction of new film thickness correlation, Int. J. Heat Mass Transf. 119 (2018) 564–576.
[16] C.Y. Zhao, W.T. Ji, Y.L. He, Y.J. Zhong, W.Q. Tao, A comprehensive numerical study on the subcooled falling film heat transfer on a horizontal smooth tube, Int. J. Heat Mass Transf. 119 (2018) 259–270.
[17] S. Jeong, S. Garimella, Falling-film and droplet mode heat and mass transfer in a horizontal tube LiBr/water absorber, Int. J. Heat Mass Transf. 45 (7) (2002) 1445–1458.
[18] L. Harikrishnan, M.P. Maiya, S. Tiwari, Investigations on heat and mass transfer characteristics of falling film horizontal tubular absorber, Int. J. Heat Mass Transf. 54 (11–12) (2011) 2609–2617.
[19] Q. Qiu, X. Zhang, S. Quan, X. Zhu, S. Shen, 3D numerical study of the liquid film distribution on the surface of a horizontal-tube falling-film evaporator, Int. J. Heat Mass Transf. 124 (2018) 943–952.
[20] H. Ding, P. Xie, D. Ingham, L. Ma, M. Pourkashanian, Flow behaviour of drop and jet modes of a laminar falling film on horizontal tubes, Int. J. Heat Mass Transf. 124 (2018) 929–942.
[21] R. Qi, L. Lu, H. Yang, F. Qin, Influence of plate surface temperature on the wetted area and system performance for falling film liquid desiccant regeneration system, Int. J. Heat Mass Transf. 64 (2013) 1003–1013.
[22] C.H. Qi, H.J. Feng, H.Q. Lv, C. Miao, Numerical and experimental research on the heat transfer of seawater desalination with liquid film outside elliptical tube, Int. J. Heat Mass Transf. 93 (2016) 207–216.
[23] X. Wang, T. Huai, Y. Li, Numerical simulation research of horizontal single-tube falling film evaporation, Procedia Eng. 205 (2017) 1500–1506.
[24] Y. Zhou, Z. Cai, Z. Ning, M. Bi, Numerical simulation of double-phase coupled heat transfer process of horizontal-tube falling film evaporation, Appl. Therm. Eng. 118 (2017) 33–40.
[25] L. Zhang, Z. Fu, Y. Liu, L. Jin, Q. Zhang, W. Hu, Experimental study on enhancement of falling film absorption process by adding various nanoparticles, Int. Commun. Heat Mass Transf. 92 (2018) 100–106.
[26] Y. Zheng, Z. Lan, K. Cao, R. Jiang, X. Ma, A new insight of temperature distribution on superhydrophilic surface horizontal tubes falling film at low spray density, Int. Commun. Heat Mass Transf. 91 (2018) 17–22.
[27] K. Huang, Y. Hu, X. Deng, Experimental study on heat and mass transfer of falling liquid films in converging-diverging tubes with water, Int. J. Heat Mass Transf. 126 (2018) 721–729.